VIBRATION FROM A RIVETING HAMMER CAUSES SEVERE NERVE DAMAGE IN THE RAT TAIL MODEL

SANDYA GOVINDA RAJU, MBBS, PhD,[1] OLAF ROGNESS, MS,[2] MAGNUS PERSSON, MS,[3] JAMES BAIN, BA,[1] and DANNY RILEY, PhD[1]

[1] Department of Cell Biology, Neurobiology & Anatomy, Medical College of Wisconsin, 8701 Watertown Plank Road, Milwaukee, Wisconsin 53226, USA

[2] Milwaukee School of Engineering, Milwaukee, Wisconsin, USA

[3] Atlas Copco Tools, Stockholm, Sweden

Accepted 10 June 2011

ABSTRACT: *Introduction*: Hand–arm vibration syndrome (HAVS) is an occupational neurodegenerative and vasospastic disorder in workers who use powered hand tools. Frequency weighting (ISO 5349) predicts little risk of injury for frequencies >500 Hz. Potentially damaging high frequencies abound in impact tool–generated shock waves. *Methods*: A rat tail impact vibration model was developed to deliver shock-wave vibration from a riveting hammer to simulate bucking bar exposure. Rat tails were vibrated continuously for 12 min. Tail flick withdrawal times were determined for noxious heat. Nerve trunks and skin were processed for light and electron microscopy. *Results*: Immediately after vibration, the tails were hyperalgesic and had disrupted myelinated axons, fragmented nerve endings, and mast-cell degranulation. By 4 days, the tails were hypoalgesic; nerve endings were lost in the skin. *Conclusions*: Shock-wave vibration causes severe nerve damage. Frequency weighting seriously underestimates the risk of nerve injury with impact tools.

Muscle Nerve **44:** 795–804, 2011

Peripheral neuropathy is a major component of hand–arm vibration syndrome (HAVS), an occupational disease that affects workers who are exposed to vibration from hand-held power tools. Hand and arm vibration causes tingling and numbness in the fingers.[1] Prolonged exposure to vibration increases the severity and persistence of HAVS symptoms.[2] Most vibration disease has been linked to *non-impact* power tools that have a major or dominant frequency in the 30–250-Hz range, and disease onset ranges from 3 to 20 years.[3–7] Workers who use *impact* tools can exhibit persistent HAVS symptoms within months of exposure.[8] The prevalence of HAVS in the aircraft industry was nearly 50% in those who had used impact riveting hammers <15 min/day for 10 years.[9] Increased vibrotactile and thermal thresholds and reduced sensory nerve conduction velocity suggest that vibration directly injures peripheral nerves, nerve endings, and mechanoreceptors.[10–12] Skin biopsies from HAVS patients have shown decreased nerve fiber density.[13–15]

The current international standard (ISO 5349) sets daily vibration exposure limits by a formula that incorporates frequency weighting. Weighting is based on subjective data that humans feel progressively less vibration for frequencies >16 Hz.[16] The formula progressively decreases risk levels so that the measured acceleration for 1.6 kHz is reduced by two orders of magnitude and is considered to contribute insignificantly to risk. Frequency weighting for risk assessment has been challenged by many researchers whose studies indicate that it underestimates the injury potential of higher frequencies and presents a false sense of security.[2,17,18] The occurrence of neural symptoms in dental hygienists who use high-speed drills and scalers that generate kilohertz vibrations contradicts the suggestion that high frequency is innocuous, although prolonged pinch gripping and wrist flexion are contributing ergonomic factors to carpal tunnel syndrome.[19] Unweighted accelerations correlate better than weighted values with vibration disease occurrence. Although exposures in the 60–800-Hz frequency range have been shown to cause neuropathology, very few studies have investigated impact vibration (shock waves), which contains major vibration energy at kilohertz frequencies.[20] For example, during riveting, the hand-held, metal bucking bar that opposes the impacts of the hammer transmits a wide bandwidth of 0.5-Hz to >8-kHz vibration energy to the fingers.[21] Bucking bar workers have a higher incidence of vibration white finger vasospasm than workers who operate the riveting gun (45% vs. 10%, respectively).[22] In this study we model bucking bar exposure by determining the effects on innervation of the rat tail of impact shock vibration generated by a riveting hammer.

Abbreviations: CGRP, calcitonin gene–related protein; HAVS, hand–arm vibration syndrome; ISO, International Organization for Standardization; PBS, phosphate-buffered saline; PGP9.5, protein gene product 9.5; ROS, reactive oxygen species

Key words: hand–arm vibration syndrome, impact tools, Langerhans cells, mast cells, skin denervation

Correspondence to: D.A. Riley; e-mail: dariley@mcw.edu

Published online 15 October 2011 in Wiley Online Library (wileyonlinelibrary.com). DOI 10.1002/mus.22206

METHODS

Animal Groups. Male Sprague-Dawley rats (275–300 g) were randomly assigned to one of four groups ($n = 8$ per group): (1) shock 0d—vibrated 12 min followed immediately by tail flick testing, tissue harvest, and then euthanasia; (2) shock 4d—vibrated, tail flick tested immediately on day 0, day

2, and day 4, tissue harvested day 4, and then euthanasia; (3) sham 0d—sham-control synchronized with shock 0d, tail flick tested, and tissue harvested; and (4) sham 4d—sham-control synchronized with shock 4d, tail flick tested immediately on day 0, day 2, and day 4, and then tissue harvested (at day 4). Rats were housed in a temperature-controlled room at 25°C and a 12-h/12-h light–dark cycle. All treatments, surgical interventions, and husbandry procedures were approved by the animal care committee of the Medical College of Wisconsin and complied with the Laboratory Animal Welfare Act.

Vibration Protocol. The vibration setup is shown in Figure 1. Rats were confined within a ventilated tube mounted to a non-vibrating platform.[23] The riveting hammer (Model RRH04P; Atlas Copco) was stabilized in a steel frame. The hammer was supplied with 20-psi air pressure, and the blow cycle was 33 Hz. A fan-shaped metal impactor (tool piece) delivered the vibration output from the hammer to the rat tail taped to the impactor platform. The position of the non-vibrating platform was adjusted so the relaxed tail was not bent, and the ventral surface of caudal vertebra 5 was completely on the impactor platform. The impactor was preloaded with 40-N compression by two bungee cords to trigger hammer cycling. The impactor acceleration measured with a laser vibrometer was $\backsim$100 m/s^2 rms (non–frequency-weighted).[24] The tail was vibrated by 12 min of continuous hammer operation. The time-frame of 12 min was chosen because it fell within the lower of the two ranges, 1–15 min[9] and 60–120 min,[8,22] for cumulative riveting hammer use per workday. Furthermore, 12 min was considered a sufficient duration to expect nerve damage, because a 4-min exposure to lithotripsy shock waves disrupts nerve fibers in rat paw skin.[25] The non-vibrating platform was separated $\backsim$1 cm from the vertically moving impactor. During hammer operation, the tail, impactor, and hammer rig were enclosed within a sound reduction box to reduce noise to <85 dB. Studies with sham control rats were run concurrently within 2 feet of the vibrated rats to control for restraint and noise. They were treated in manner similar to that of vibrated rats, except the tails were taped to a non-vibrating impactor. The immediate (0d) groups were euthanized 10–15 min after completing vibration/sham-vibration exposure and tail flick testing. The survival groups were returned to their cages and allowed to recover for 4 days before tissue removal and euthanasia.

Tail Flick Response Test. In each measurement session, the dorsal skin of the proximal tail region of the rats in all four groups was stimulated by a noxious heat lamp (EMDIE Instrument Co., Maidens, Virginia). On the first day of vibration, each rat was placed in a tube cage, and the time interval for the rat to withdraw (flick) the tail away from the heat was measured before vibration exposure to define the individual baseline response. A pair of vibrated and sham-vibrated rats in their individual tubes were then positioned for the 12-min exposure to either vibration or mock vibration. Immediately after 0d vibration or sham-vibration exposure, the second tail flick test was performed. The heat source was preset to maintain a constant intensity for all rats and timed-out at 8 s to avoid overheating injury. Tail flick testing was performed after vibration on days 0, 2, and 4 for the treated and sham-control rats in the survival groups.

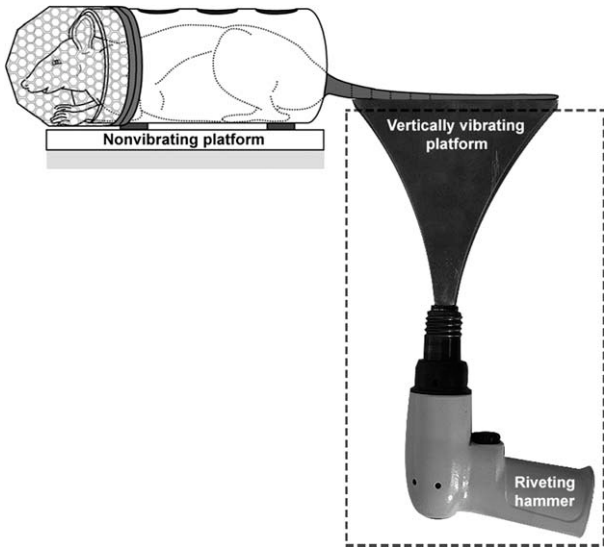

FIGURE 1. Rat tail model of shock-wave vibration exposure. The awake rat is confined to the cage on the non-vibrating platform with its tail taped to the top of a fan-shaped steel plate that is vertically accelerated by a riveting hammer (Atlas Copco). The hammer and most of the plate are enclosed in a sound-reduction box (dotted line).

Tissue Processing. Rats were anesthetized with ketamine (72 mg/kg), xylazine (12 mg/kg), and acepromazine (0.09 mg/kg) injected intramuscularly. The tail skin covering segments C5–7 was incised ventrally to mark the region that had directly contacted the vibration platform. After a complete circular incision proximal to C5, the incision margins were gripped by two hemostats to pull the skin off the tail as a unit. The isolated skin "tube" was cut into short tubular pieces that were immersion-fixed in 4% paraformaldehyde for 2.5 h, cryoprotected in graded sucrose-buffered solutions, and frozen in liquid nitrogen. Proximal tail segment 7 was excised and immersion fixed in 4% glutaraldehyde and 2% paraformaldehyde for 2.5 h before overnight storage at 2°–5°C in the 0.1 M cacodylate

buffer. The left and right ventrolateral nerve trunks were removed from the segment and post-fixed in 1.3% osmium tetroxide for 2 h before buffer rinsing and conventional embedding in epoxy-resin.[20,26,27]

Morphometric Analysis of the Nerve Trunks. The embedded nerves were semithin sectioned at 0.5 μm and stained with toluidine blue for morphometric analysis. The total number of myelinated axons in each nerve cross-section was counted, and the percentage of axons with disrupted myelin was determined using ImageJ v1.28 software (NIH). As in previous studies, disrupted myelin was defined when both darker staining with toluidine blue and two or more focal areas of widening of the myelin were present.[20,26,27] Disrupted myelinated nerve fibers cannot be quantitated solely on the basis of toluidine blue staining intensity. Representative regions of the sham, shock 0d, and shock 4d group nerves were examined at the electron-microscopic level to assess nerve fiber damage. Nerve edema was defined as an increase over sham in the area between myelinated axons in $\times$40 images of semithin cross-sections of nerves.[26] The interaxonal area was measured by employing the exclusion thresholding procedure of MetaMorph v5.2 (Universal Imaging Corp., West Chester, Pennsylvania).

Nerve fiber diameter (axon plus myelin), myelin thickness, and axon diameter of the myelinated fibers contained completely within $\times$100 optical fields were measured using ImageJ v1.28 software (153 ± 6 myelinated axons per rat, $n = 24$ rats). Non-biased selection of the measurement fields (average 3.3 ± 0.4 fields per rat) was performed by positioning randomly with the $\times$4 objective, because at low magnification the details of individual nerve fibers cannot be resolved. Magnification was then increased to the $\times$100 objective field, and measurements were started if the axons were oriented in cross-section, large blood vessels were not present to lower the axon count, and sectioning artifacts were not present. From these measurements, the G ratio (axon diameter divided by fiber diameter) was calculated for each nerve fiber.[28]

Staining Skin Nerve Fibers, Langerhans Cells, and Mast Cells. The frozen skin samples were cryosectioned into cross-sections (40 μm thick) for incubation free floating in staining media followed by mounting on glass slides (Fisher SuperFrost Plus). Sections from vibrated and sham rats were stained together in adjacent drops under identical conditions to control for incubation conditions and timing. Fluorescence photomicrographs were taken with an epifluorescence microscope (Optiphot-2; Nikon, Tokyo, Japan) fitted with appropriate excitation and barrier filters and a digital camera (SPOT RT3; Diagnostic Instruments, Sterling Heights, Michigan).

All nerve fibers supplying the skin were visualized by pan-neuronal immunostaining with antibodies against protein gene product 9.5 (PGP9.5). PGP9.5 is advertised as a neuronal-specific, C-terminal ubiquitin hydrolase that removes ubiquitin adducts, the proteasome degradation targeting signal, from proteins.[29] PGP9.5 antibodies have been utilized to assess innervation patterns in multiple studies of normal, injured, and diseased tissues.[14,25,30,31] More recently, PGP9.5 and other neuronal proteins were shown to be expressed in Langerhans cells.[32] Langerhans cells are phagocytic cells in the dermis involved in skin immune reactions, and they are intimately associated with terminal nerve fibers.[33] To distinguish PGP9.5 nerve immunostaining from Langerhans cells immunolabeling, sections were doubled-labeled with PGP9.5 and OX-6, a specific immunomarker for Langerhans cells. Another major cell type in the skin is the mast cell. Initially, we utilized a rabbit polyclonal antibody for PGP9.5 (Ultraclone, UK) that required signal amplification by biotinylated secondary antibody and avidin-conjugated fluorophore, tertiary labeling. It is not well known that avidin binds strongly to mast-cell granules.[34] The amplification technique fluorescently labeled both nerve fibers (PGP9.5 positive) and mast cells (avidin-conjugated fluorophore positive), making it difficult to characterize changes in each cell type without the confusion from overlapping labeling. This confounder was eliminated by switching to an alternative, high-affinity monoclonal antibody against PGP9.5 that was imaged with a secondary fluorescently tagged antibody (red, DyLight 549). After PGP9.5 immunostaining, the secretory granules of mast cells were selectively stained in drops for 1 h at room temperature with avidin-conjugated AlexaFluor 488 (Invitrogen, Madison, Wisconsin) diluted 1:1000.[34]

Details of Immunostaining. Immunostaining was initiated with a blocking step solution consisting of 1$\times$ phosphate-buffered saline (PBS, pH 7.2) containing either 5% normal goat serum or 5% normal donkey serum, 1% bovine serum albumin, and 0.3% Triton X-100. Free-floating sections were immersed in drops of solutions in 1.1-cm circular wells (75 μl) created in a Parafilm sheet cut to fit within a 9-cm plastic Petri dish. The bottom of the dish contained hydrated paper creating a humidified chamber, with the dish lid in place to prevent solution drying. Samples were blocked for 1 h at room temperature. Subsequently, free-floating sections were transferred with fine forceps to drops containing various primary antibodies diluted in

blocking solution and incubated at 2°–5°C in a refrigerator. Primary antibodies were omitted for the negative controls. The primary antibodies used were mouse anti-PGP9.5 at 1:1200 (MCA-BH7, EnCor Biotechnology, Gainesville, Florida) and mouse anti–OX-6 at 1:80 (MCA46R; AbD Serotec, Raleigh, North Carolina). The anti-PGP9.5 antibody was incubated for 2 days in a refrigerator (2°–5°C). One-day incubation was sufficient for the OX-6 primary antibody. After primary antibody incubation and rinsing (three times, 10 min) in 1× PBS, sections were incubated for 1 h at room temperature in secondary fluorescent antibodies diluted 1:400 in 1× PBS (goat anti-mouse DyLight 488 or goat anti-mouse DyLight 549). Different fluorescent color wavelengths were used in combinations suited for double labeling with primary antibodies. Fluorescently labeled structures were best visualized as dark structures when the color images were converted to gray scale and inverted images with Adobe Photoshop.

Statistical Analysis. A two-way, repeated-measures analysis of variance (treatment × day) was performed to compare the tail flick responses. One-way analysis of variance was used to compare means for myelin fiber disruption, myelin thickness, G ratio, and axon diameter, followed by Student–Newman–Keuls testing. Differences were considered significant at $P < 0.05$. Values are presented as mean ± SEM.

RESULTS

Behavioral Evaluation. During vibration, the rats were monitored for signs of stress, including increased vocalization, startle responses, excessive movement within the restraint tube, efforts to withdraw the tail from the vibrating platform during vibration, and periorbital porphyrin secretion. Neither the sham nor the vibration groups demonstrated these signs in response to the noise or the shock-wave vibration.

Tail Flick Response Test. The pretreatment tail flick response latencies averaged 4.5 ± 0.4 s for the sham and 4.8 ± 0.3 s for the shock-vibration groups (Fig. 2). In the sham 4d group, the tail flick response times did not deviate significantly from baseline through the 4 days. The shock 0d and 4d rats, however, demonstrated significantly shorter response times immediately after vibration, with a mean latency of 2.9 ± 0.3 s (Fig. 2). At 2 days post-vibration, the response times averaged 3.6 ± 0.5 s in the shock 4d vibrated rats and were not different from the pretreatment values. By day 4, the response times rose to 5.8 ± 0.6 s in the shock 4d rats. This was significantly higher than the pre-treatment and sham 4d values.

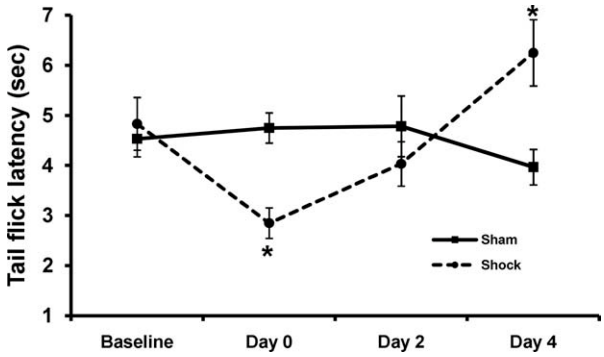

FIGURE 2. Tail flick withdrawal latency to noxious heat was assessed on multiple days in the sham 4d control and shock 4d vibrated rats before (baseline), immediately after 12-min exposure to vibration (day 0), after 2-day recovery (day 2), and after 4-day recovery (day 4). Compared with baseline, latency was significantly (*$P < 0.05$) shorter on day 0. After 2 days of recovery, vibrated and sham were not different. By day 4 post-vibration, the latency was significantly (*$P < 0.05$) longer than that of baseline.

Nerve Trunk Myelin Disruption and Edema. The average myelin disruption and edema for the sham 0d and sham 4d rats were not statistically different, so the rats were combined into one sham control group. The ventrolateral nerve trunks contained, on average, 1326.5 ± 56.5 myelinated nerve fibers per cross-section. In the sham group, the majority of myelinated axons had moderately stained, compact normal myelin, and 13.6 ± 0.6% of fibers exhibited myelin darker staining and widening (Fig. 3A). The dark staining and widening of myelin in the sham group represented sections through normal nodes of Ranvier and Schmidt–Lanterman clefts with pockets of Schwann cell cytoplasm into which the toluidine blue stain penetrated. In the shock 0d and 4d rats, the higher percentages of axons with darkly stained myelin were due to delamination of myelin (Figs. 3B and C and 4). Schwann-cell hypertrophy was common in the shock 4d rats. The percentage of disrupted fibers (28.7 ± 1.1%) in the shock 0d group was double that of the sham group ($P < 0.001$) (Fig. 3A and B). Four days after shock-vibration exposure, a significantly ($P < 0.001$) higher percentage of nerve fibers, 35.1 ± 1.4%, exhibited myelin damage (Fig. 3A–C and 4).

The myelinated fibers of the nerve trunks ranged in diameter from 3 to 13 μm in the vibrated and sham rats. To ascertain whether vibration damaged a particular size of nerve fiber, the fibers were sorted into diameter bins of small (3.0–5.9 μm), medium (6.0–8.9 μm), and large (≥9.0 μm). The percentages of small, medium, and large fibers in the shock 0d and 4d groups were not significantly ($P \geq 0.17$) different from those in the sham group. The average myelin thickness, however, was significantly increased immediately after

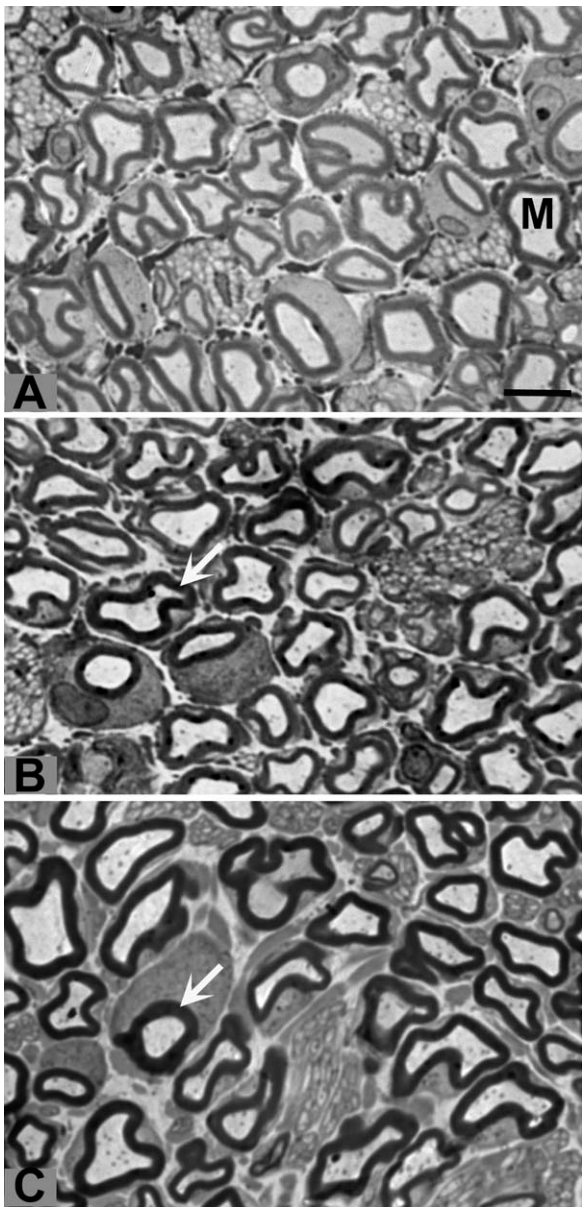

FIGURE 3. Toluidine blue–stained, semithin cross-sections of the ventrolateral tail nerve trunks. The majority of the myelinated axons (M) in the sham 0d rats have compact myelin that is uniformly moderately stained **(A)**. The shock 0d **(B)** and shock 4d **(C)** nerves contain higher percentages of axons with darkly stained myelin and focally widening (arrows). Bar in **(A)** = 10 μm (same for all panels).

shock vibration, with more myelin widening at 4 days post-exposure (Table 1). Myelin thickening in small and medium fibers was greater than sham immediately after vibration (shock 0d) (Table 1). All fiber sizes had significant increases in myelin thickness in the shock 4d survival group (Table 1). Shock vibration decreased the G ratio in all three size groups at 4 days post-vibration (Table 2). Axon diameters of the medium and large myelinated fibers in the shock 4d groups were significantly smaller than in the sham group, and the

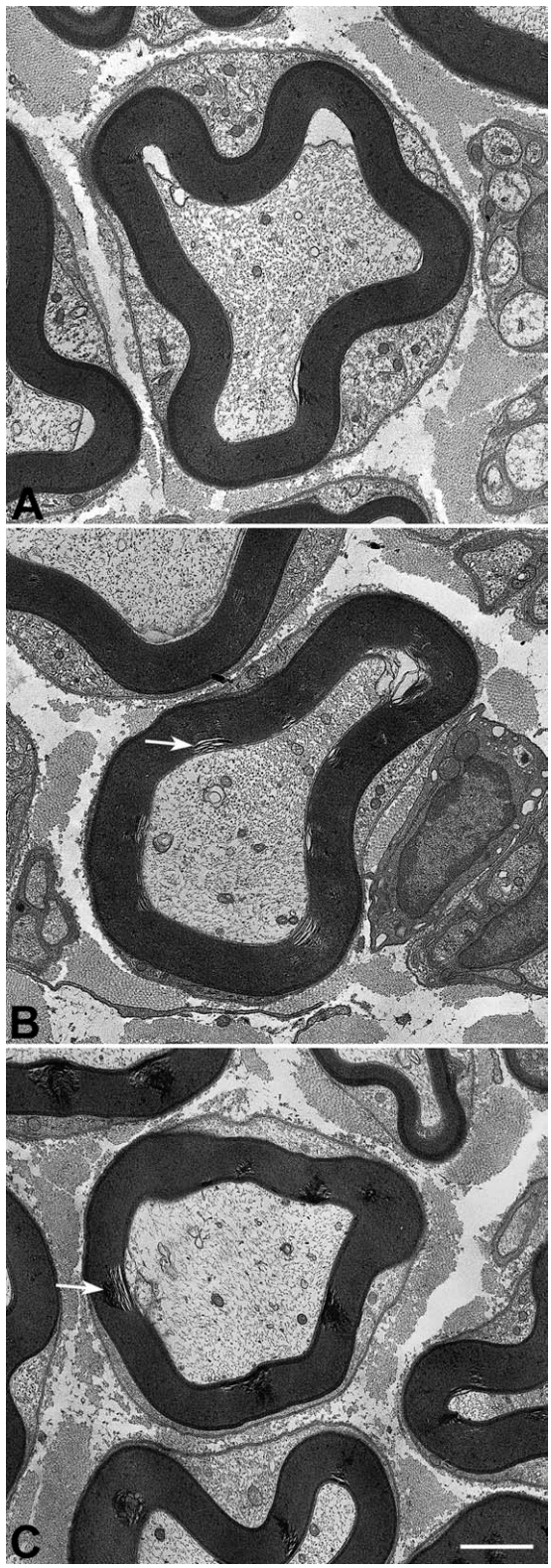

FIGURE 4. Representative electron-microscopic images of myelinated axons in the ventral nerve trunks of the sham, shock 0d, and shock 4d rats. Compared with sham control, the myelin of the vibrated nerves exhibits multiple sites (arrows) of delamination disruption. Bar = 1.4 μm.

Table 1. Vibration increases myelin thickness.

Nerve fiber size	Myelin thickness (μm)		
	Sham	Shock 0d	Shock 4d
Small fibers	0.64 ± 0.02	0.75 ± 0.03*	0.81 ± 0.04†
Medium fibers	0.90 ± 0.03	1.02 ± 0.02*	1.22 ± 0.03‡,§
Large fibers	1.08 ± 0.04	1.19 ± 0.04	1.39 ± 0.07*,§
All fibers	0.90 ± 0.05	1.03 ± 0.02*	1.23 ± 0.05‡,§

Values are expressed as mean ± SEM. Sham: mock vibrated simultaneously with vibrated rats; shock 0d: vibrated 12 min and biopsied immediately after tail flick testing; shock 4d: vibrated 12 min and biopsied 4 days later.
**$P < 0.05$, †$P < 0.01$, and ‡$P < 0.001$ (significant difference) vs. sham.*
§$P < 0.01$ (significant difference) vs. shock 0d.

medium-sized fibers had smaller axon diameters than the shock 0d immediate group (Table 3).

Shock vibration produced immediate intraneural edema as evidenced by the increase in percentage of intraneural area. Compared with the sham percent area (11.8 ± 1.2%), the shock 0d (18.1 ± 0.8%) and 4d (20.2 ± 1.5%) groups showed significant ($P < 0.01$) elevations.

Skin Structure and Cell Distribution. The skin of the tail has regular bands of epidermal scales alternating with interscale regions from which hairs emerge in trios and project over the scale (Fig. 5). The scales were about 800 μm long, and the interscale regions were about 200 μm wide, so this ring pattern repeated at 1-mm intervals. When assessing nerve fiber properties, comparisons were made in similar regions, because the cellular distribution and characteristics varied between regions.

The interscale regions contained high concentrations of Langerhans cells in the sub-epidermal region, the junction between the epidermis and dermis.[35] These cells were most abundant surrounding the emerging hair shafts, and they diminished in number under the scales (Fig. 6). Double immunostaining with PGP9.5 and OX-6 revealed that Langerhans cells were in close contact with nerve fibers and that the Langerhans cells exhibited weak immunoreactivity for PGP9.5.

Table 2. Shock vibration decreases G ratios of myelinated nerve fibers.

Nerve fiber size	G ratio (axon diameter ÷ nerve fiber diameter)		
	Sham	Shock 0d	Shock 4d
Small fibers	0.74 ± 0.01	0.71 ± 0.01	0.67 ± 0.02*
Medium fibers	0.75 ± 0.01	0.74 ± 0.01	0.68 ± 0.01†,§
Large fibers	0.78 ± 0.01	0.76 ± 0.01	0.72 ± 0.01†,‡
All fibers	0.76 ± 0.01	0.74 ± 0.01	0.69 ± 0.01†,§

Sham: mock vibrated in simultaneously with vibrated rats; shock 0d: vibrated 12 min and biopsied immediately after tail flick testing; shock 4d: vibrated 12 min and biopsied 4 days later.
**$P < 0.01$ and †$P < 0.001$ (significant difference) vs. sham.*
‡$P < 0.05$ and §$P < 0.01$ (significant difference) vs. shock 0d.

Table 3. Vibration reduces the axon diameter of myelinated fibers.

Nerve fiber size	Axon diameter (μm)		
	Sham	Shock 0d	Shock 4d
Small fibers	3.70 ± 0.05	3.58 ± 0.05	3.63 ± 0.06
Medium fibers	5.78 ± 0.07	5.60 ± 0.23	5.25 ± 0.07†,‡
Large fibers	7.85 ± 0.07	7.62 ± 0.17	7.27 ± 0.10*

Sham: mock vibrated in simultaneously with vibrated rats; shock 0d: vibrated 12 min and biopsied immediately after tail flick testing; shock 4d: vibrated 12 min and biopsied 4 days later.
**$P < 0.01$ and †$P < 0.001$ (significant difference) vs. sham.*
‡$P < 0.05$ (significant difference) vs. shock 0d.

Cutaneous Nerve Endings—PGP9.5 Nerve Immunoreactivity. In the sham group, PGP9.5 immunostaining of the skin showed a high density of nerve fibers immediately below the epidermis and surrounding the individual hair follicles at the level of the sebaceous glands (Figs. 6A and 7A). Hair innervation is characteristic of the vellus hair palisade pattern, comprised of lanceolate mechanoreceptors and multimodal, circumferential free nerve endings.[36,37] The nerve fibers in focus in the inverted fluorescence images appeared as continuous dark lines. In contrast, 4 days after shock vibration there were fewer immunoreactive nerve fibers. Those remaining were lighter stained and exhibited a discontinuous pattern of irregularly sized granules, suggestive of necrosis and phagocytosis of the damaged endings (Figs. 6B and 7B). Immediately after vibration in the shock 0d skin, the immunostained axons appeared as discontinuous and enlarged dark staining segments. This pattern indicated acutely fragmented and swollen axons.

Mast Cells. In the sham group, mast cells in the mid-dermis encircled hair follicles and exhibited very low levels of degranulation in the lateral and dorsal regions of the skin (Fig. 8A). Degranulation was extensive in the deepest layer of the dermis in

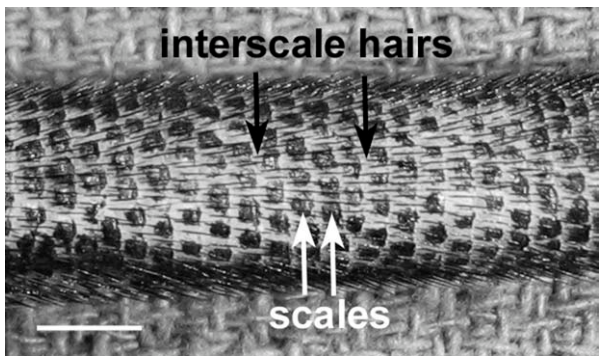

FIGURE 5. Dorsal view of the skin on segment C6 of the rat's tail. The epidermal scales (white arrows) and the hairs have been blackened with a pen to reveal detail. The transverse rows of scales are separated by interscale regions (black arrows) from which the hairs emerge. Bar = 4 mm.

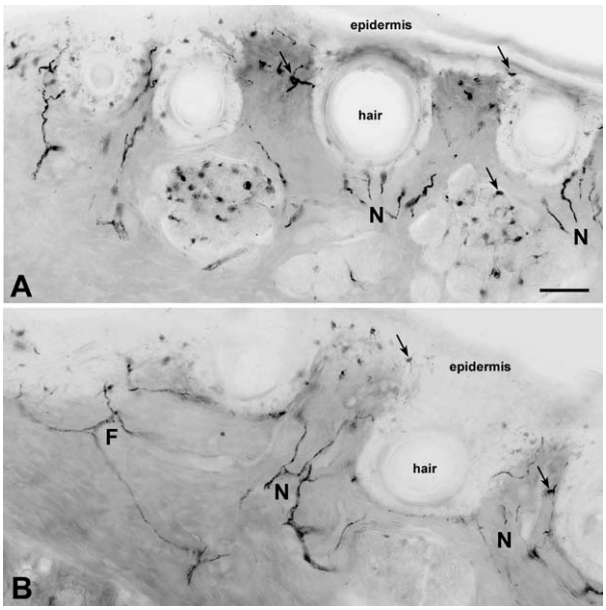

FIGURE 6. Cross-sections through the interscale regions of the skin of sham **(A)** and shock 4d **(B)** rat tails. Nerve fibers (N) and Langerhans cells (arrows) are immunoreactive for PGP9.5 antibodies. The immunofluorescence image is inverted, so immunostained structures appear dark. In the sham-control skin, the immunoreactive nerve fibers course through the dermis and arborize in the sub-epidermal plexus around the hairs. Nerve fibers in the shock 4d skin are less numerous, have lighter staining, and exhibit a granular structure indicative of degeneration as compared with the dark and continuous structure of the intact fibers in the sham. The Langerhans cells are small stellate cells residing in the subdermal region and the sebaceous glands deep to the hairs. The nerve fibers and Langerhans cells were distinguished by double staining the same sections with OX-6 antibody specific for Langerhans cells (not shown). Bar = 70 μm.

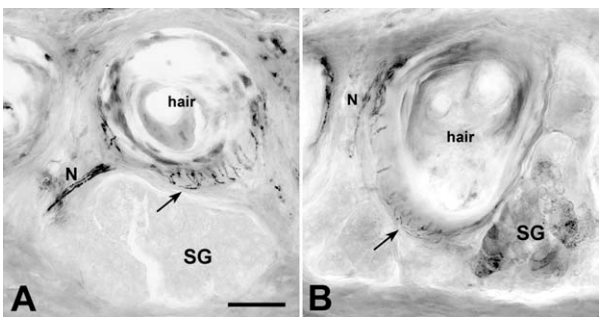

FIGURE 7. The PGP9.5 immunoreactive nerve fibers in the mid-dermis region approach the hair follicle in a nerve bundle (N), and the nerve endings arborize (arrows) longitudinally as lanceolate endings on the outer sheath of the follicles. In the sham control **(A)**, the nerve bundle contains darkly immunoreactive fibers, and the nerve endings form numerous fine dark networks. The nerve bundle in the shock 4d vibrated skin **(B)** contains lightly immunoreactive and indistinct degenerated fibers. The nerve endings are also lightly immunoreactive and less numerous compared with sham. The sebaceous glands (SG) for sham are tinted at background levels. The sebaceous glands for shock 4d are moderately to darkly immunostained with peppery dark granules, suggestive of the degeneration of their innervation. Bar = 70 μm.

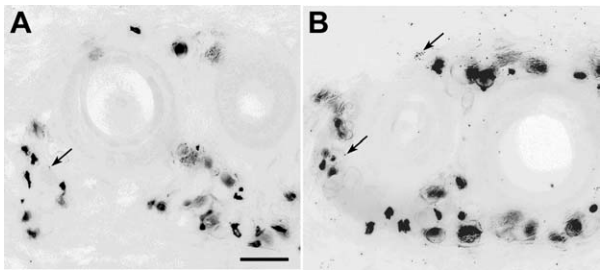

FIGURE 8. Clusters of mast cells surround the hair follicles in the mid-dermis regions of the sham **(A)** and shock 0d **(B)** rats. The mast cells are darkly stained with avidin-conjugated fluorophore (inverted image). In the sham, occasional mast-cell granules (arrow) are present extracellularly. The number of released mast-cell granules (arrows) is much higher immediately after 12-min vibration. Bar = 70 μm.

both the sham and vibrated rats. The mechanical strain of stripping the skin from the tail during dissection caused this massive degranulation. In the shock 0d skin, marked mast-cell degranulation occurred around the hair follicles in the mid-dermis, consistent with vibration-induced release (Fig. 8B). In the shock 4d skin, mast-cell degranulation in the mid-dermis had returned to the sham control level.

DISCUSSION

Exposing the rat tail to high-acceleration, shock-wave vibration for 12 min produces dramatic functional and structural changes indicative of immediate nerve injury and extensive degeneration of the cutaneous innervation by 4 days. Sensory perception of noxious heat stimulation is heightened immediately after vibration exposure but becomes hyporesponsive 4 days later. Immediately after vibration, PGP9.5 immunostaining of terminal nerve fibers in the skin changes from continuous to fragmented, indicating physical disruption. The immediate hyperalgesia to heat is consistent with the damaged sensory nerve endings being hypersensitized by tissue injury–generated inflammatory substances, such as mast-cell–released histamine.[38]

The rat tail impact vibration model not only damages axons rapidly, but the calm behavior of the rats during vibration indicates a lack of awareness that injury is occurring. Interestingly, humans who operate a variety of power hand tools are unable to perceive when the level of acceleration is unsafe.[39] The failure to sense nerve damage during vibration further validates our impact vibration animal model to simulate the worker's fingers holding a bucking bar on the rivet while it is impacted by a riveting gun.

Within the ventrolateral nerve trunks immediately after shock vibration, there is a higher-than-normal percentage of axons with disrupted myelin, and the percentage increases by 4 days. Progression of myelin damage after stopping vibration was observed previously for sinusoidal vibration.[20] The duty or impact cycle of the riveting hammer was

33 Hz. Our studies of 30-, 60-, and 120-Hz sinusoidal (non-impact) vibration show that frequencies in this range cause immediate vasoconstriction of the rat tail artery and reduction of skin and nerve blood flow.[40] This mimics vibration white finger (vasospasm) in humans.[8] Reduced blood flow and reflow generate reactive oxygen species (ROS). The free radicals may contribute to disruption of myelin and intraneural edema in the nerve trunks.[26,41] The shrinkage of the axons of myelinated fibers in the ventrolateral nerve trunks in the shock 4d group is suggestive of retrograde atrophy secondary to the loss of terminal nerve fibers and endings in the skin. Impact vibration decreases the G ratios of the small, medium, and large myelinated axons. This indicates that the impact vibration damages and degrades the functions of all sizes of myelinated fibers (Aδ-Aβ) rather than a subset. The decreased G ratio and myelin disruption contribute to reduced and aberrant nerve conduction velocity.[28,42] The hypoalgesia in shock 0d rats is similar to that in workers with HAVS who develop higher thresholds to heat and touch. The delayed tail flick withdrawal reflex at 4 days may also involve damage to alpha motor fibers because tail withdrawal requires contraction of intrinsic and extrinsic skeletal muscles. Weakness of the hand and forearm muscles occurs in HAVS.[43] The change in noxious thermal sensitivity indicates that non-myelinated C fibers are also damaged. The functional and structural changes within the nerve trunks and the loss of sensory nerve endings in the skin appear to explain the hypoalgesia present 4 days after shock vibration. In humans, the destruction and reinnervation of PGP9.5-immunoreactive fibers in the skin correlates directly with the loss and subsequent return of heat and touch sensitivity.[44] The rat tail impact vibration model is amenable to the study of the mechanism of axon loss, because altered function and severe neurodegeneration occur in minutes and days.

In our previous studies, hyper- and hypoalgesia were not observed after sinusoidal vibration delivered in a continuous pattern for 4 h.[27] Structurally, the nerve trunks exhibited myelin disruption and interstitial edema. This suggests that these two neuropathologies are not sufficient to cause the sensitivity changes observed in the tails exposed to shock vibration. In the present study, disrupted myelin was found during both hyperalgesia and hypoalgesia, revealing that the increased and decreased sensitivities do not correlate with the myelin disruption and edema.

The temporal pattern of loss of PGP9.5 immunostaining after impact shock vibration is consistent with lithotripsy shock-wave destruction of the cutaneous innervation of rat skin.[25] The time scenario for axon loss in the rat is also similar to the degeneration of nerve endings found after 3–5 days in human skin after sural nerve denervation.[31] Finger skin biopsies of workers with HAVS with numbness have fewer axons visualized by PGP9.5 and calcitonin gene–related protein (CGRP) immunostaining and electron microscopy.[14,15] The destruction of the innervation in this study was throughout the tail skin. If the damage had been limited to the ventral region in direct contact with the impactor, physical trauma would explain the nerve injury. There were no visible abrasions of the ventral skin. The circumferential pattern of loss is consistent with shock waves entering the tail ventrally, propagating circumferentially, and disrupting the cutaneous terminal nerve fibers and endings. Shock waves cause cavitation in water and generate microbubbles that burst and release shock-wave energy that destroys cell membrane integrity.[45] Why was the nerve destruction greater in the skin than in the ventrolateral nerve trunks? The myelinated axons in the nerve trunks exhibited myelin disruption, axon shrinkage, and intraneural edema, but there was no loss of axons at 4 days based on myelinated axon counts. The nerve trunks lie deep to the long tendon bundles, which may protect (shield) the nerve fibers from shock waves. The physics of acoustic high-frequency (mHz) ultrasound waves has been studied extensively. These waves are known to reflect back at sites of increased tissue acoustic impedance, which is the basis of ultrasonographic imaging. Tissue acoustic impedance is the product of tissue density $\times$ the speed of sound in that tissue. In the rat tail, impedance increases are expected at two interfaces: (1) the cellular epidermis and the dense collagen/elastin-rich matrix of the dermis; and (2) the dermis and very dense collagen bundles of long tendons. Thus, the shock-wave energy is postulated to reflect back from these deep tissues into the superficial layers and damage the superficial nerve fibers. When the rat sciatic nerve and skin were exposed to lithotripter-generated shock waves, the axons in the skin were destroyed, but those in the nerve were minimally damaged.[13,25] The dense collagen wrapping of the sciatic nerve was suggested to reflect the shock waves away from the axons. The postulated propagation patterns of the impact shock waves in the tail may account for the damage to terminal nerve endings and relative sparing of the axons in the nerve trunks.

Clinical Implications. To lower the risk to workers, further studies are necessary to determine which aspects of impact vibration, such as acceleration, duration, or frequency content, cause the neuropathologies. The high acceleration of the impactor ($\backsim$100 m/s^2 rms) may account for the immediate mast-cell degranulation and rapid and severe nerve

damage, because vibration disease in humans is directly related to vibration magnitude. Collateral damage of the kidney parenchyma is an undesirable side effect during lithotripter fragmenting of renal stones, and injury severity is directly dependent on the magnitude of the shock waves delivered.[46] Reducing the shock-wave exposure rate from 120 to 60/min greatly decreased renal damage.[46] In this study, the riveting hammer delivered a shock wave with each blow cycle for a total of 23,760 shock waves. Redesigning tools with slower duty cycles to reduce shock-wave number may decrease the prevalence of HAVS in workers; however, the tool may function less efficiently at the lower rate and require longer use. Longer use is undesirable, because HAVS occurrence is directly correlated with the duration of tool use.[1,2] The daily use of riveting hammers varies tremendously in different work situations. From the literature, we estimate that riveters operate the hammer in bursts lasting 1–60 s, depending on the project.[8,9,17,22] By the end of the 8-h workday, total tool use may be as brief as 1 min or as long as 2 hours. The onset of HAVS is months rather than years when daily exposure is high.[8,9] Herein we have examined the effects of a single 12-min exposure to impact vibration. Delivering the same total exposure in a pattern of 1 min/day over 12 days may have generated more neuropathology, because multiple exposures produced a more long-lasting degeneration than a single exposure from an extracorporeal shock-wave therapy machine.[47]

Some aspects of vibration injury may be frequency-dependent. The very high-frequency (kHz) components of the shock waves[9] may be more damaging than the 30–250-Hz vibration characteristic of non-impact tools. Impact tool use can produce HAVS in months, whereas non-impact tools typically require years to cause disease.[3,5–8] Workers who use their bare hands to guide the chisel of an impact chipper or the socket from a nut runner tool develop vibration white finger in that hand.[17] Workers holding the bucking bar develop HAVS at a higher rate compared with riveting hammer operators.[22] The hand needs protection against shock waves. ISO 10819–compliant, anti-vibration gloves that absorb frequencies at 500 Hz and higher may protect against high-frequency injury, but further studies are necessary.[48] Our findings indicate that the practice of frequency weighting seriously underestimates the risk potential of high-frequency vibration components.

This work was supported by a grant from the National Institute for Occupational Safety and Health (R01 OH003493).

REFERENCES

1. Friden J. Vibration damage to the hand: clinical presentation, prognosis and length and severity of vibration required. J Hand Surg [Br] 2001;26:471–474.
2. Griffin MJ, Bovenzi M, Nelson CM. Dose-response patterns for vibration-induced white finger. Occup Environ Med 2003;60:16–26.
3. Barregard L. Short daily exposure to hand-arm vibrations in Swedish car mechanics. Appl Occup Environ Hyg 2003;18:35–40.
4. Futatsuka M, Shono M, Sakakibara K, Quoc Quian P. Hand arm vibration in tropical rain forestry workers. Cent Eur J Public Health 1995;3:90–92.
5. Palmer K, Inskip H, Martyn C, Coggon D. Symptoms of hand-arm vibration syndrome in gas distribution operatives. Occup Environ Med 1998;55:716–721.
6. Wasserman DE, Taylor W. Lessons from hand-arm vibration syndrome research. Am J Ind Med 1991;19:539–546.
7. Yamamoto H, Zheng KC, Ariizumi M. A study of the hand-arm vibration syndrome in Okinawa, a subtropical area of Japan. Ind Health 2002;40:59–62.
8. Gurdjian ES, Walker LW. Traumatic vasospastic disease of the hand (white fingers). JAMA 1945;129:668–672.
9. Dandanell R, Engstrom K. Vibration from riveting tools in the frequency range 6 Hz–10 MHz and Raynaud's phenomenon. Scand J Work Environ Health 1986;12:338–342.
10. Brismar T, Ekenvall L. Nerve conduction in the hands of vibration exposed workers. Electroencephalogr Clin Neurophysiol 1992;85: 173–176.
11. Giannini F, Rossi S, Passero S, Bovenzi M, Cannavˋ G, Mancini R. Multifocal neural conduction impairment in forestry workers exposed and not exposed to vibration. Clin Neurophysiol 1999;110: 1276–1283.
12. Sakakibara H, Hirata M, Hasiguchi T, Toibana N, Koshiyama H, Zhu SK, et al. Digital sensory nerve conduction velocity and vibration perception threshold in peripheral neurological test for hand-arm vibration syndrome. Am J Ind Med 1996;30:219–224.
13. Wu YH, Liang HW, Chen WS, Lai JS, Luh JJ, et al. Electrophysiological and functional effects of shock waves on the sciatic nerve of rats. Ultrasound Med Biol 2008;34:1688–1696.
14. Goldsmith PC, Molina FA, Bunker CB, Terenghi G, Leslie TA, Fowler CJ, et al. Cutaneous nerve fibre depletion in vibration white finger. J R Soc Med 1994;87:377–381.
15. Takeuchi T, Fatatsuka M, Imanichi H, Yamada S. Pathological changes observed in the finger biopsy of patients with vibration-induced white finger. Scand J Work Environ Health 1986;12:280–283.
16. Griffin MJ. Minimum health and safety requirements for workers exposed to hand-transmitted vibration and whole-body vibration in the European Union; a review. Occup Environ Med 2004;61: 387–397.
17. Engstrom K, Dandanell R. Exposure conditions and Raynaud's phenomenon among riveters in the aircraft industry. Scand J Work Environ Health 1986;12:293–295.
18. Nilsson T, Burnstõm L, Hagberg M. Risk assessment of vibration exposure and white fingers among platers. Int Arch Occup Environ Health 1989;61:473–481.
19. Cherniack M, Brammer AJ, Nilsson T, Lundstom R, Meyer JD, Morse T, et al. Nerve conduction and sensorineural function in dental hygienists using high frequency ultrasound handpieces. Am J Ind Med 2006;49:313–326.
20. Govindaraju SR, Curry BD, Bain JLW, Riley DA. Nerve damage occurs at a wide range of vibration frequencies. Int J Ind Ergon 2008;38:687–692.
21. Pelmear PL, Leong D, Taylor W, Nagalingam M, Fung D. Measurement of vibration of hand-held tools: weighted or unweighted? J Occup Med 1989;31:902–908.
22. McKenna KM, McGran S, Blann AD, Allan JA. An investigation into the acute vascular effects of riveting. Br J Ind Med 1993;50:160–166.
23. Curry BD, Bain JL, Yan JG, Zhang LL, Yamaguchi M, Matloub HS, et al. Vibration injury damages arterial endothelial cells. Muscle Nerve 2002;25:527–534.
24. Xu X, Riley DA, Persson M, Welcome DE, Krajnak K, Govindaraju SR, et al. Characterizing impact vibration for rat tail vibration exposure experiments. In: Wilder DG, editor. 3rd American Conference on Human Vibration. Iowa City, IA: University of Iowa Press; 2010.
25. Ohtori S, Inoue G, Mannouji C, Saisu T, Takahashi K, Chiba T, et al. Shock wave application to rat skin induces degeneration and reinnervation of sensory nerve fibres. Neurosci Lett 2001;315:57–60.
26. Govindaraju SR, Curry BD, Jain JL, Riley DA. Effects of temperature on vibration-induced damage in nerves and arteries. Muscle Nerve 2006;33:415–423.
27. Govindaraju SR, Curry BD, Jain JL, Riley DA. Comparison of continuous and intermittent vibration effects on rat tail artery and nerve. Muscle Nerve 2006;34:197–204.
28. Chomiak T, Hu B. What is the optimal value of the g-ratio for myelinated fibers in the rat CNS? A theoretical approach. PLoS One 2009;4:e7754.
29. Schofield JN, Day IN, Thompson RJ, Edwards YH. PGP9.5, a ubiquitin C-terminal hydrolase; pattern of mRNA and protein expression

during neural development in the mouse. Brain Res Dev Brain Res 1995;85:229–238.
30. Ebenezer GJ, Hauer P, Gibbons C, McArthur JC, Polydefkis M. Assessment of epidermal nerve fibers: a new diagnostic and predictive tool for peripheral neuropathies. J Neuropathol Exp Neurol 2007;66:1059–1073.
31. Ebenezer GJ, McArthur JC, Thomas D, Murinson B, Hauer P. Denervation of skin in neuropathies: the sequence of axonal and Schwann cell changes in skin biopsies. Brain 2007;130:2703–2714.
32. Hamzeh H, Guadillèr A, Sabido O, Tchou I, Lambert C, Schmitt D, et al. Expression of PGP9.5 on Langerhans' cells and their precursors. Acta Derm Venereol 2000;80:14–16.
33. Siau C, Xiao W, Bennett GJ. Paclitaxel- and vincristine-evoked painful peripheral neuropathies: loss of epidermal innervation and activation of Langerhans cells. Exp Neurol 2006;201:507–514.
34. Tharp MD, Seelig LL Jr, Tigelaar RE, Bergstresser PR. Conjugated avidin binds to mast cell granules. J Histochem Cytochem 1985;33: 27–32.
35. Schweizer J, Marks F. Lack of relationship between Langerhans cells, epidermal cell proliferation and epidermal G1 chalone. Experientia 1978;34:1235–1237.
36. Halata Z. Sensory innervation of the hairy skin (light- and electronmicroscopic study. J Invest Dermatol 1993;101(suppl):75S–81S.
37. Kaidoh T, Inoue T. N-cadherin expression in palisade nerve endings of rat vellus hairs. J Comp Neurol 2008;506:525–534.
38. Mobarakeh JI, Sakurada S, Katsuyama S, Kutsuwa M, Kuramasu A, Lin ZY, et al. Role of histamine H(1) receptor in pain perception: a study of the receptor gene knockout mice. Eur J Pharmacol 2000; 391:81–89.
39. Vergara M, Sancho J-L, Rodriquez P, Perez-Gonzalez A. Hand-transmitted vibration in power tools: Accomplishment of standards and users' perception. Int J Indust Ergon 2008;38:652–660.
40. Curry BD, Govindaraju SR, Bain JL, Zhang LL, Yan JG, Matloub HS, et al. Evidence for frequency-dependent arterial damage in vibrated rat tails. Anat Rec A Discov Mol Cell Evol Biol 2005;284: 511–521.
41. Bizzozero OA, DeJesus G, Howard TA. Exposure of rat optic nerves to nitric oxide causes protein S-nitrosation and myelin decompaction. Neurochem Res 2004;29:1675–1685.
42. Loffredo MA, Yan JG, Kao D, Zhang LL, Matloub HS. Persistent reduction of conduction velocity and myelinated axon damage in vibrated rat tail nerves. Muscle Nerve 2009;39:770–775.
43. Bylund SH, Ahlgren C. Experiences and consequences for women with hand-arm vibration injuries. Work 2010;35:431–439.
44. Nolano M, Simone DA, Wendelschafer-Crabbe G, Johnson T, Hazen E, Kennedy WR. Topical capsaicin in humans: parallel loss of epidermal nerve fibers and pain sensation. Pain 1999;81:135–145.
45. Sems A, Dimeff R, Iannotti JP. Extracorporeal shock wave therapy in the treatment of chronic tendinopathies. J Am Acad Orthop Surg 2006;14:195–204.
46. Connors BA, Evan AP, Blomgren PM, Handa LK, Willis LR, Gao S, et al. Extracorporeal shock wave lithotripsy at 60 shock waves/min reduces renal injury in a porcine model. BJU Int 2009;104: 1004–1008.
47. Takahashi N, Ohtori S, Saisu T, Moriya H, Wada Y. Second application of low-energy shock waves has a cumulative effect on free nerve endings. Clin Orthop Relat Res 2006;443:315–319.
48. Dong RG, McDowell TW, Welcome DE, Warren C, Wu JZ, Rakheja S. Analysis of anti-vibration gloves mechanism and evaluation methods. J Sound Vibration 2009;321:435–453.